

A GRAVITATIONAL DOUBLE SCATTERING MECHANISM FOR GENERATING HIGH VELOCITY OBJECTS

JOHAN SAMSING¹

Draft version August 24, 2021

ABSTRACT

We present a dynamical model describing how halo particles can receive a significant energy kick from the merger between their own host halo and a target halo. This is highly relevant for understanding the growth of cosmological halos, and could especially provide an explanation for some high velocity objects. The model we present includes a *double scattering mechanism*, where a halo particle is given a significant energy kick by undergoing two subsequent gravitational deflections during the merger. The first deflection is by the potential of the target halo, whereas the second is by the potential of the particle's original host halo. The resultant energy kick arises because the two halos move relative to each other during the two deflections. To our knowledge, this mechanism has never been characterized in this context before. We derive analytically a halo particle's total kick energy, which is composed of energy from the double scattering mechanism and energy release from tidal fields, as a function of its position in its original host halo. In the case of a 1 : 10 merger between two Hernquist halos, we estimate that the presented mechanisms can generate particles with a velocity ~ 2 times the virial velocity of the target halo measured at its virial sphere. This motivates us to suggest that the high velocity of the recently discovered globular cluster HVCG-1 (Caldwell et al. 2014) can be explained by a head-on halo merger. Finally, we illustrate the orbital evolution of particles outside the virial sphere of the target halo, by solving the equation of motion in an expanding universe. We find a 'sweet spot' around a scale factor of 0.3–0.5 for ejecting particles into large orbits, which easily can reach beyond ~ 5 virial radii.

1. INTRODUCTION

Several high velocity objects on seemingly unbound orbits have been observed, ranging from stellar objects (Brown et al. 2014; Zheng et al. 2014), supernovae (SNe) (Gal-Yam et al. 2003; Sand et al. 2011) and gamma ray burst (GRBs) (Fong et al. 2013; Tunnicliffe et al. 2014; Boylan et al. 2014) to more extended systems like globular clusters (GCs) (Peng et al. 2011; Caldwell et al. 2014) and dwarf galaxies (Majewski et al. 2007; Chapman et al. 2007). In many of these cases the origin of the velocity kick is unknown, but several mechanisms have been suggested. One is binary-single interactions where the binding energy of a binary is dynamically released into a third object, which thereby can escape with high velocity (Heggie 1975). These interactions are believed to have a non-negligible chance of happening especially between stellar objects (Sigurdsson & Phinney 1993; Gvaramadze et al. 2009) and stars encountering either single or binary black hole (BH) systems (Hills 1988; Yu & Tremaine 2003; Bromley et al. 2006). Several observations indicate in fact that stellar interactions with the supermassive black hole (SMBH) at the center of our galaxy, is a likely explanation for some local high velocity stars (Gualandris et al. 2005; Brown et al. 2012). More extended objects like GCs are probably not kicked by BH binary interactions, due to the high probability for disruption, however the outcome from such an interaction is still uncertain (Caldwell et al. 2014). Dark matter (DM) subhalo interactions on the other hand, is able to kick extended objects up to ~ 2 times the virial velocity of the host halo without major disruptions, as indicated by numerical simulations (Sales et al. 2007; Ludlow et al. 2009). High velocity stars can also arise from isolated binaries if the heavier member undergoes a violent mass loss, a channel first suggested by Blaauw (1961) to explain the high number of "run away" O-B stars. More exotic kick mechanisms for describing host-

less stellar remnants, pulsars, and possible hyper velocity BHs have been suggested as well, from the role of asymmetric GW radiation (Bekenstein 1973; Fitchett 1983; Redmount & Rees 1989; Pietilä et al. 1995; Davies et al. 2002) to the asphericity of supernovae explosions (Burrows & Hayes 1996; Burrows et al. 2007; Janka 2012).

Unbound particles have also been discussed from a cosmological perspective. Recent studies (Behroozi et al. 2013) illustrate that $\sim 10\%$ of all the DM at the virial radius is in fact unbound. Luminous matter with no specific host halo has also been observed in especially galaxy clusters, a component known as intra cluster light (ICL). This has been extensively studied both through observations (e.g. Zwicky 1951; Guenou et al. 2012; Presotto et al. 2014) and numerically (Willman et al. 2004), and is believed to be a direct consequence of the dynamical evolution of galaxies including tidal stripping and mergers (Moore et al. 1996). Theoretical attempts have also been made to understand the final distribution of particles in DM halos. This includes models from spherical collapse (e.g. Bertschinger 1985; Dalal et al. 2010) to statistical mechanics (e.g. Ogorodnikov 1957; Lynden-Bell 1967; Spiegel & Hernquist 1992; Hansen et al. 2005; Hjorth & Williams 2010; Pontzen & Governato 2013). Especially concerning the unbound and high velocity component, recent work by Teyssier et al. (2009); Joyce et al. (2009); Carucci et al. (2014) show that high velocity particles in mergers are likely generated through rapid mean field changes in the potential. This was also noted by Abadi et al. (2009) who further proposed a direct connection to the observed population of high velocity B-type stars.

Data from upcoming surveys like *LSST*² and especially *Gaia*³ will in the near future also measure positions and velocities for more than ~ 150 million stars with unprecedented precision. This not only offers unique possibilities for map-

¹ Dark Cosmology Centre, Niels Bohr Institute, University of Copenhagen, Juliane Maries Vej 30, 2100 Copenhagen, Denmark

² <http://www.lsst.org/lsst/>

³ <http://sci.esa.int/gaia/>

ping out the current Milky Way potential and its past evolution (e.g. Zhao et al. 1999; Peñarrubia et al. 2012; Price-Whelan et al. 2014; Sanderson et al. 2014), but will also make it possible to make detailed studies of the past dynamical interactions (Gualandris et al. 2005). A central question could here be if the Milky Way in its past had a SMBH binary dynamically interacting with the environment. Detections of high velocity objects are here again playing a central role.

In this paper we present a new dynamical mechanism for explaining how halo particles gain a significant energy kick during the merger between their initial host halo and a target halo. It is well known that halo mergers produce an unbound component (e.g. Hernquist 1992; Teysier et al. 2009; Carucci et al. 2014), but no clear dynamical explanation has been given yet. In this work we seek to give such an explanation. Besides a well understood energy change from tidal fields (also present in stellar disruption events (Kochanek 1994)), we show that an additional mechanism play a significant role in changing the energy of the halo particles. The new mechanism we present is a double scattering mechanism, where a given particle receives a significant energy kick by undergoing two deflections during the merger. We derive analytically the energy kick for two merging Hernquist halos (Hernquist 1990), but the idea of the mechanism is not limited to this scenario. For instance, we note that a very similar mechanism has been described within heavy nuclei interactions where an electron can be ejected into the continuum (unbound orbit) or captured by a passing nucleus (dynamical capture) by undergoing a double collision⁴(Thomas 1927; Shakeshaft & Spruch 1979).

The paper is organized in the following way: In Section 2 we first give an introduction to the dynamical processes playing a role in halo mergers which include tidal fields and our proposed double scattering mechanism. Section 3 describes our numerical simulations, initial conditions, and the halo merger examples we consider in this paper. The energy release from tidal fields is described in Section 4 and the double scattering mechanism is presented in Section 5. In both of these sections we derive the energy change of a given particle as a function of its position in its initial host halo. In Section 6 we shortly describe observable consequences and show how a kick energy translates to an observable velocity excess. In Section 7 we explore how far a dynamically kicked particle can travel after leaving the virial sphere of its target halo, by solving the equation of motion in an expanding universe. Conclusions are given in Section 8.

2. ENERGY OF PARTICLES DURING HALO MERGERS

The energy of individual halo particles can change significantly during a merger between their initial host halo (H_2) and a larger target halo (H_1). Some particles will lose energy and become bound to the target halo H_1 , whereas some will gain energy and escape with relatively high velocity. In this section we introduce the dynamical mechanisms responsible for changing the energy of each individual particle initially bound to the incoming halo H_2 .

2.1. Dynamical Mechanisms

We first consider Figure 1, which shows an N-body simulation of a merger between two DM halos. The incoming halo

⁴ The quantum-mechanical solution to this interaction was not found until 1955 (Drisko 1955), due to the fascinating fact that the second Born term is here dominating over the first because of the double scattering nature, or two-step process, of the problem.

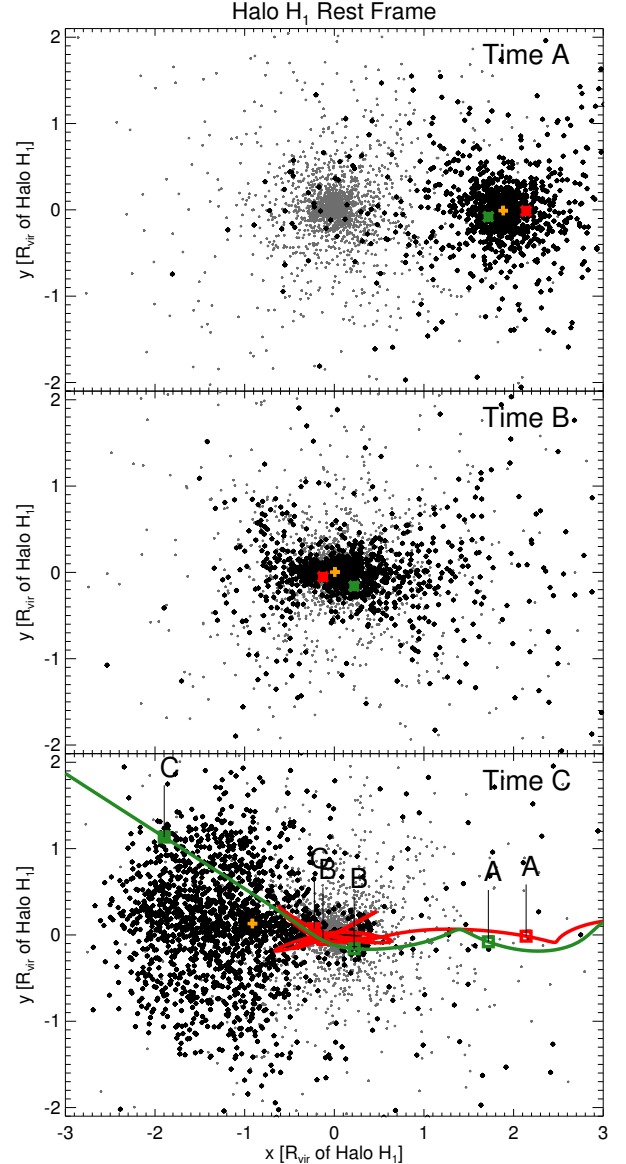


FIG. 1.— Illustration of a 1 : 10 merger between two DM halos merging with the escape velocity of the target halo. The particles in the smaller incoming halo are shown in *black*, while the particles of the larger target halo are shown in *grey*. The panels from *top to bottom* show three different times (A,B,C) of the merger. In the bottom panel the full trajectories of two selected particles are also shown. The *green* particle gains a positive energy kick during the merger and is thereby escaping the system, whereas the *red* particle loses energy and becomes bound to the target halo. The *orange* symbol shows a particle which is located within 5% of the virial radius of the smaller incoming halo at all times prior to the merger. This illustrates a luminous galactic component. The merger clearly separates the three highlighted particles in both position and velocity. As described in Section 2, this separation can be explained by two separate dynamical processes: The first involve tidal fields (Section 4) and the second is our proposed double scattering mechanism (Section 5). Properties of the green particle are shown in Figure 3 and 4.

H_2 approaches from the right on a radial orbit with a velocity equal to the escape velocity of the target halo. The orange symbol shows a particle which at all times prior to the merger is located within 5% of the incoming halo's virial radius. This symbol can therefore represent a luminous galactic component (Kravtsov 2013). On the figure is also highlighted the orbits of two particles: The green particle receives a positive energy change through the merger and can thereby escape,

whereas the red particle gets bound as a result of a negative energy change. The differences in final energy between the orange, green, and red particles arise due to a series of dynamical mechanisms, which to first order can be separately considered. Each of these change the energy of the particles as described in the following.

The first energy change arises because the potential of the target halo H_1 is not constant across the profile of the incoming halo H_2 . As a result, the particles in H_2 located on the side closest to H_1 have less energy than the particles located on the far side. This energy difference increases as the distance between the two halos decreases, i.e., a subject particle will gradually gain or lose energy as the two halos approach each other. This continues until H_2 is tidally disrupted by the tidal field of H_1 . We denote the final energy change from this process by ΔE_{TF} , where TF is short for tidal field.

The second energy change arises from our proposed double scattering mechanism, where a given particle is first deflected by H_1 and then subsequently by H_2 . This generates a change in energy because the two halos move relative to each other during the two deflections. We denote the energy change from this process by ΔE_{DS} , where DS is short for double scattering. To our knowledge, this contribution has not been characterized before and will therefore be the main topic of this paper.

The third and last energy change happens after the double scattering, as the particles are moving away from H_2 along their new orbits. As the particles are climbing out of the potential of H_2 their velocity decreases, which results in an energy change in the frame of H_1 due to the relative motion between H_1 and H_2 . For particles escaping the merger remnant the energy change will be negative, as we will illustrate. We denote the final energy change from this process by ΔE_{esc} .

2.2. Total Energy Change

The dynamical mechanisms we consider in this work can, to first order, be considered separately and not affecting the motion of a given particle at the same time. The total energy change ΔE_{tot} a given particle will experience, can therefore be expressed by the sum of the individual energy contributions

$$\Delta E_{tot} \approx \Delta E_{TF} + \Delta E_{DS} + \Delta E_{esc}. \quad (1)$$

For particles receiving a high energy kick the first two terms will usually be positive and the last negligible. In this paper we therefore focus on calculating the contribution from ΔE_{TF} and ΔE_{DS} . A numerical example of how the three energy terms individually change the total energy of a particle during a merger is shown in the bottom panel of Figure 3. The details of this figure will be described later.

3. GENERAL SETUP

We model the two merging halos H_1 and H_2 by Hernquist (HQ) profiles (Hernquist 1990), with an anisotropy parameter $\beta = 0$. In this case the mass profile is given by

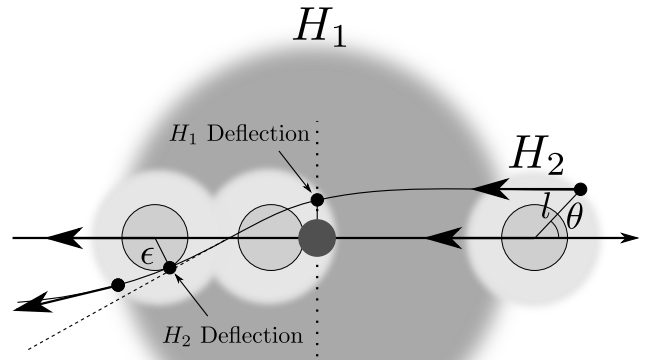
$$M_i(r) = M_i \frac{(r/a_i)^2}{(1+r/a_i)^2}, \quad (2)$$

and the corresponding gravitational potential by

$$\Phi_i(r) = -\frac{GM_i}{a_i} \frac{1}{(1+r/a_i)}, \quad (3)$$

where M_i is the total mass of halo i , r is the distance from the halo center, $M_i(r)$ is the mass enclosed by r , $\Phi(r)$ is the

Halo H_1 Rest Frame



Halo H_2 Rest Frame

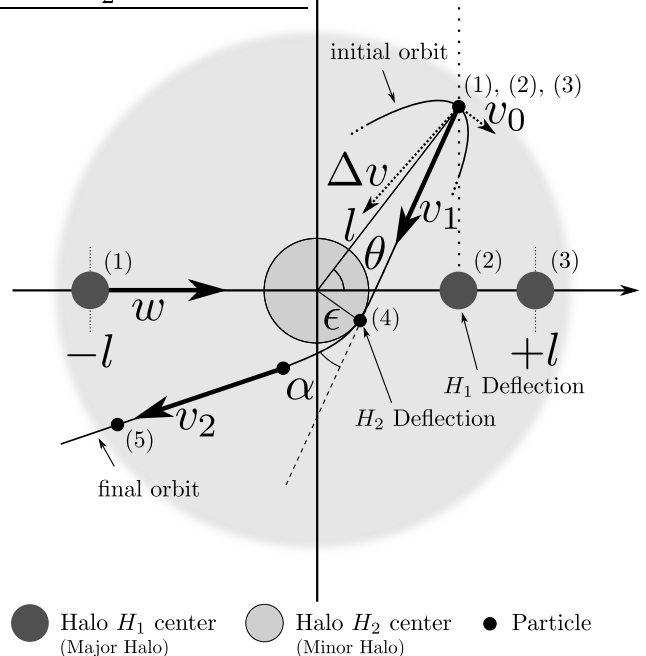


FIG. 2.— Schematic illustration of a particle (black dot) gaining energy during the merger between its original host halo H_2 (light grey) and a target halo H_1 (dark grey). The top plot shows the orbital trajectory of the particle in the rest frame (RF) of H_1 , while the bottom plot shows the trajectory in the RF of H_2 . As illustrated, the particle undergoes two separate deflections during its orbit: The first is by the momentarily dominating potential of H_1 , whereas the second is by the potential of its original host halo H_2 . The deflection by H_1 results in a velocity kick $\Delta \mathbf{v}$ of the particle in the RF of H_2 , as illustrated in the bottom plot. The energy of the particle is conserved during this deflection in the RF of H_1 , but not in the RF of H_2 . Due to the induced $\Delta \mathbf{v}$, the particle now travels through H_2 , where it scatters off the central parts of H_2 at a peri-center distance $\sim \epsilon$. The energy of the particle during this deflection is conserved in the RF of H_2 , but not in the RF of H_1 , because H_1 and H_2 are moving relative to each other. As a result of the two deflections, the particle gains an energy kick ΔE_{DS} in the RF of H_1 . The numbers from (1-5) on the two paths represent simultaneous positions of the particle and H_1 .

potential at distance r and a is a characteristic scale radius. In the following, we occasionally use units of a_1 and we use a prime to denote this, e.g., $x' \equiv x/a_1$. We also find it useful, to write down the radial velocity between H_1 and a particle moving in its potential on a radial orbit

$$w^2(r) = -2\Phi_1(r) + w^2(0) + 2\Phi_1(0), \quad (4)$$

where $w(r)$ is the radial velocity of the particle at distance r . We will use this relation to calculate the relative velocity between halo H_1 and the incoming halo H_2 . The estimate for $w(r)$ in the above equation (4) ignores the effect from dynamical friction, which causes H_2 to lose orbital energy by exchanging momentum with the surrounding particles in H_1 (Chandrasekhar 1943). Dynamical friction actually plays a minor role in our case because $\Delta E_{DS} \propto w$, as we describe in Section 5, but for now we ignore it to simplify the analysis. For the following analyzes, we further assume that the two halos merge with zero impact parameter and that the mass of the target halo H_1 is much larger than the incoming halo H_2 , i.e. $M_1 \gg M_2$. This mass hierarchy is relevant for the growth of cosmological halos, that are believed to build hierarchically by hundreds of minor mergers (Fakhouri et al. 2010).

The N-body simulations presented throughout the paper are performed using Gadget II (Springel 2005), with the two HQ halos set up in equilibrium by Eddington’s Method (Eddington 1916) using a well tested code previously used for studying the anisotropy in halo mergers (Sparre & Hansen 2012a,b). The halo concentration $c_i \equiv R_{i,\text{vir}}/a_i$ is set to 5 for both halos and the virial radius $R_{i,\text{vir}}$ is calculated by requiring the density inside the halo to be 200 times the mean density of the universe at redshift $z = 2$ (Wechsler et al. 2002; Mo et al. 2010). We fix the merger mass ratio at 1 : 10 for all simulations and the incoming halo H_2 is set to have zero energy relative to the target halo H_1 , which corresponds to a velocity at infinity $w_\infty = 0$. These initial conditions are typical in a cosmological perspective (Prada et al. 2012), however a wide range of both encounter velocities and impact parameters are seen in full cosmological simulations (Wetzel 2011).

4. ENERGY FROM TIDAL FIELDS

The first energy change the particles in H_2 experience is from tidal fields. This change arises, because the particles in H_2 all have the same bulk velocity $w(r)$, but experience different values of Φ_1 due to their different spatial positions in H_2 . The difference in Φ_1 across H_2 increases as the two halos approach each other and the particles are therefore released with a wide spread in energy at the time H_2 tidally disrupts. This scenario is very similar to stellar disruption events (see e.g. Kochanek (1994)). In this section we derive an estimate for the energy change ΔE_{TF} a given particle in H_2 will experience from this process, as a function of the particle’s position in H_2 just prior to the merger.

4.1. Evolution of Particle Energy Before Merger

We consider a particle located in H_2 , with orbital velocity \mathbf{v} and polar position l, θ measured in the rest frame (RF) of H_2 . The configuration is illustrated in Figure 2. The energy of the particle in the RF of H_1 before the merger, is given by

$$E(l, \theta, r) = \frac{1}{2}w(r)^2 + \Phi_1(r) + \frac{1}{2}v^2 + \Phi_2(l) + \mathbf{w} \cdot \mathbf{v} + \Delta\Phi_1(l, \theta, r), \quad (5)$$

where r is the distance between H_2 and H_1 , w is the corresponding relative velocity and $\Delta\Phi_1$ is the difference between the value of Φ_1 at the position of the center of mass (CM) of H_2 and the particle, respectively. The first two terms equal the CM energy of H_2 in the RF of H_1 , where the next two terms equal the energy of the particle in the RF of H_2 , i.e., the sum of the first four terms remains approximately constant, as the two halos approach each other. The fifth term $\mathbf{w} \cdot \mathbf{v}$ is by contrast oscillating between positive and negative values as

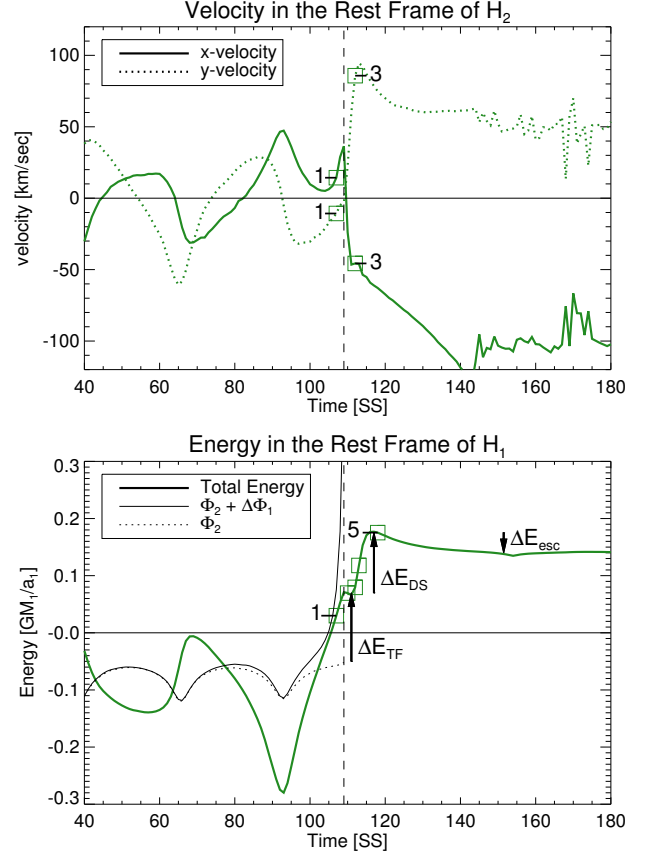


FIG. 3.— Velocity and energy as functions of time for a particle gaining a positive energy through the merger. The particle is the same as shown in Figures 1 and 4. The vertical dashed line indicates the time when the two merging halos pass each other. *Top*: Horizontal and vertical velocity of the particle in the RF of its original host halo H_2 as a function of time. The numbered squares (1,3) indicate when H_2 passes H_1 from $-l$ to $+l$ as illustrated in Figure 2. As seen, the particle gains a significant velocity kick $\Delta \mathbf{v}$ during this passage, as discussed in Section 5.2.1. *Bottom*: Energy of the particle in the RF of H_1 as a function of time. The first energy increase (ΔE_{TF}) is due to the variation of Φ_1 across H_2 , as discussed in Section 4, whereas the second energy increase (ΔE_{DS}) is generated through our proposed double scattering mechanism, discussed in Section 5. The gradual energy decrease (ΔE_{esc}) at later times is happening, because the particle is dragged back as it travels out of H_2 , which itself moves relative to H_1 . Comparing with Figure 4, we see that the second increase happens when the particle undergoes its ‘second deflection’ by H_2 . This is in complete agreement with our double scattering model.

the particle orbits H_2 . Energy can be released from this term, but the contribution is random and does not simply add to the other energy contributions for reasons we will not discuss here. The only term that changes the energy of the particle in a constructive way is the last term $\Delta\Phi_1$, which is given by

$$\begin{aligned} \Delta\Phi_1(l, \theta, r) &= \frac{\Phi_1(0)}{1 + \sqrt{r'^2 + l'^2 + 2l'r'\cos(\theta)}} - \frac{\Phi_1(0)}{1 + r'}, \\ &\approx \Phi_1(0) \frac{l'\cos(\theta)}{(1+r')^2}, \quad r' \gg l'. \end{aligned} \quad (6)$$

This illustrates that the change in energy of the particle due to the variation of Φ_1 across H_2 , scales to linear order as $\sim l\cos(\theta)/r^2$, i.e., particles in H_2 located on the side closest to H_1 lose energy as H_2 approaches H_1 , whereas particles on the other side instead gain energy.

The energy contribution from the $\Delta\Phi_1$ term is seen in the bottom panel of Figure 3, which shows the energy of the green particle from Figure 1 as a function of time. One can see that

the $\Delta\Phi_1$ term does not contribute when r is large (at early times), but as r decreases and becomes comparable to l , the $\Delta\Phi_1$ term clearly increases and the total energy of the particle therefore increases as well. This energy increase continues, until the particle tidally detaches from H_2 and starts to move completely under the influence of H_1 (just before the vertical dashed line). The moment at which this happens, can be estimated by comparing the tidal force exerted on the particle F_{tid} by H_1 with the binding force F_{bin} by H_2 (Read et al. 2006). These force terms are simply given by $F_{tid} = GM_1(d)/d^2 - GM_1(r)/r^2$ and $F_{bin} = GM_2/l^2$, where d denotes the distance from H_1 to the particle. By defining the force ratio $\delta_{TF} \equiv F_{tid}/F_{bin}$, one can now relate δ_{TF} and the position of the particle in H_2 to a corresponding distance between the two halos R_{TF} . In the case of two HQ halos we find to linear order,

$$R'_{TF} \approx \delta_{TF}^{-1/3} [2l' \cos(\theta)(d'_2 + l')^2 M_1/M_2]^{1/3} - 1, \quad r' \gg l'. \quad (7)$$

If $\delta_{TF} = 1$, then the corresponding R_{TF} will be the standard definition of the tidal radius.

4.2. Resultant Energy From Tidal Fields

The resultant energy change ΔE_{TF} of the particle induced by the tidal field of H_1 , is given by evaluating the potential energy difference $\Delta\Phi_1$ (equation (6)) at distance R_{TF} (equation (7)) where the particle tidally detaches from H_2 ,

$$\Delta E_{TF}(l, \theta, R_{TF}) \approx \Delta\Phi_1(l, \theta, r = R_{TF}(\delta_{TF})). \quad (8)$$

A fair agreement with numerical simulations is found when $\delta_{TF} \approx 3-5$. However, we also find slight deviations which primarily are caused by the difficulties in defining a representative R_{TF} . To do a better estimation, one needs to include the possibility for the particle to detach gradually, but this is highly non trivial. A gradual detachment is, e.g., seen in the energy evolution of the particle shown in Figure 3. For clarity, we therefore instead report the energy change ΔE_{TF} the particle has received, when the two halos are separated by the distance $r = l$ (denoted by '1' in Figure 3). The corresponding energy is both accurately determined and representative for the resultant energy change ΔE_{TF} induced by Φ_1 . We find this to be true for the majority of the particles in our simulation. The right panel in Figure 5 shows $\Delta E_{TF}(l, \theta, r = l)$ as a function of the position of the particle in H_2 . We see that the change in energy is estimated to be around $0.1 - 0.2\Phi_1(0)$ and the maximum kick is given to particles just behind the center of H_2 . The tidal field contribution ΔE_{TF} is also illustrated and discussed in Figure 3.

5. ENERGY FROM THE DOUBLE SCATTERING MECHANISM

The second energy change the particles in H_2 experience during the merger is generated by the double scattering mechanism. In this section we describe the kinematics of the mechanism and derive an analytical solution for the resulting kick energy ΔE_{DS} . As seen in Figure 3, the energy contributions from tidal fields and the double scattering mechanism are of the same order. The mechanism is therefore playing an important role for how energy is distributed in halo mergers.

5.1. Origin of the Double Scattering Kick Energy

The double scattering mechanism is a process where a particle is gravitationally deflected two times during the merger between its own host halo H_2 and a target halo H_1 . The first

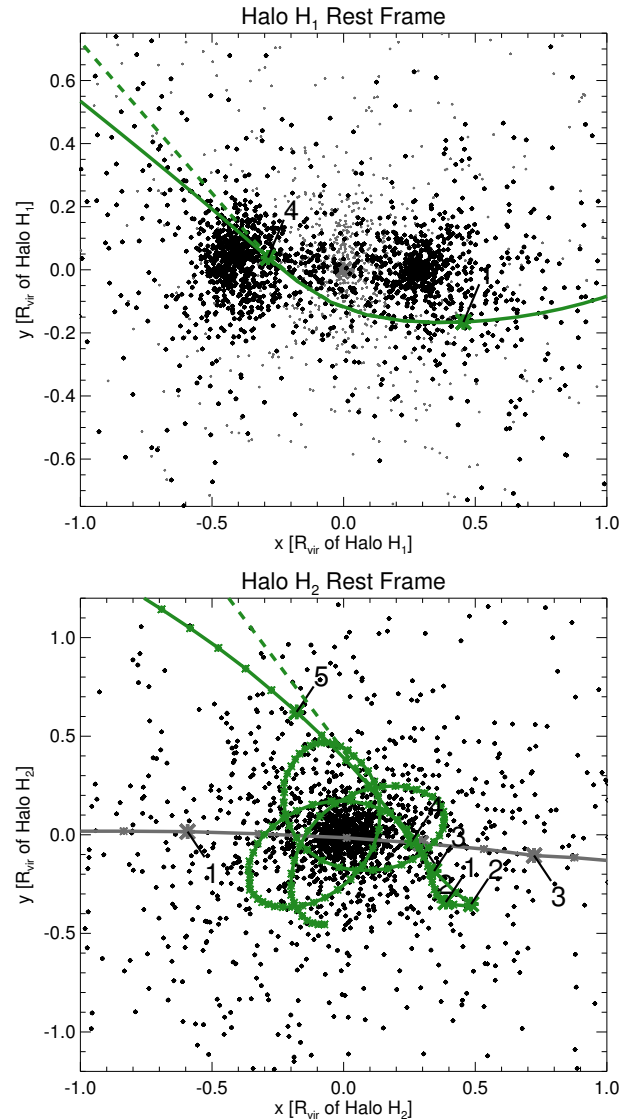


FIG. 4.— Orbital trajectory of a halo particle (green) gaining a significant energy kick from the merger between its own initial host halo H_2 (black) and a target halo H_1 (grey). The particle is the same as the green one shown in Figure 1. The green solid lines show the full orbit of the particle, whereas the green dashed lines show the orbit if the particle is not undergoing its 'second deflection' by H_2 . This second deflection directly leads to the energy kick ΔE_{DS} generated by the double scattering mechanism, as described in Section 5.2. The dashed line would therefore lead to no energy increase from this mechanism. The numbers refer to five important moments as illustrated in Figure 2. *Top*: Orbit of the particle in the RF of H_1 . The halo particles of H_2 are plotted at time 1 (right halo) and 4 (left halo), respectively. *Bottom*: Orbit of the particle in the RF of H_2 . The horizontal grey line shows the orbit of the target halo H_1 that moves from left to right. The smaller stars on the orbits indicate equal time intervals. The angle between the solid and the dashed line is denoted by α , and is calculated in equation (14). The corresponding time dependent velocity and energy of the particle are shown in Figure 3.

deflection is by the potential of H_1 , which momentarily dominates as the two halos overlap, whereas the second is by the potential of H_2 , which can dominate after the two halos have passed each other. We refer to the deflection by H_1 as the 'first deflection' and the subsequent deflection by H_2 as the 'second deflection'. The two merging halos are moving relative to each other during the merger, so the two deflections are therefore happening in two different velocity frames. The energy of the particle during each deflection is conserved in the frame of deflection, but because the two frames move relative

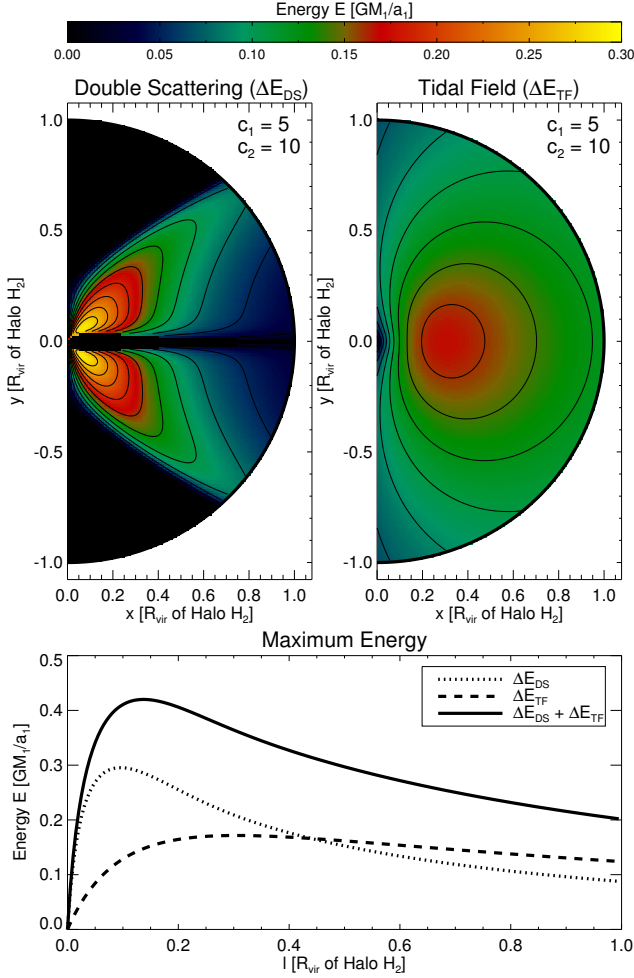


FIG. 5.— Dynamical kick energy generated by tidal fields (ΔE_{TF} , section 4) and by our proposed double scattering mechanism (ΔE_{DS} , Section 5), as a function of particle position in H_2 just prior to the merger. The results are for a 1 : 10 head-on merger between two HQ halos with concentrations, $c_1 = 5$ and $c_2 = 10$, passing each other with the escape velocity of H_1 . *Top*: Contour plots showing our theoretical calculated kick energy as a function of the position of the particle in H_2 just prior to the merger. The *left* plot shows the contribution from tidal fields ΔE_{TF} , where the *right* plot shows the contribution from the double scattering mechanism ΔE_{DS} (using $1.5\Delta v_y$ to correct for the known bias as explained in Section 5.2.3). The two plots only show the right hand side ($x_p > 0$) of the incoming halo H_2 , which in this example is approaching H_1 from right to left. Particles with $x_p > 0$ will gain the illustrated energy, whereas particles with $x_p < 0$ instead will lose this energy. This follows trivially from our analytical estimates. *Bottom*: The maximum kick energy as a function of the distance l of the particle from the CM of H_2 . As one can see, the maximum kick energy from the two mechanisms is around $\sim 0.4\Phi_1(0)$. This will lead to particles with a velocity around two times the virial velocity of the target halo H_1 , as discussed in Section 6.

to each other, a deflection in one frame can result in an energy change in the other. In our case, the deflection by H_2 changes the velocity of the particle by an amount δv along the motion of the two merging halos. The particle energy is constant in the frame of H_2 , but in the frame of H_1 the energy changes by an amount $\sim (\delta v + w)^2 - w^2 \sim \delta v w$. This is the contribution from the double scattering mechanism, denoted by ΔE_{DS} . A schematic illustration is shown in Figure 2, where a numerical example is shown in Figure 4. In the following, we calculate the details of this double scattering process.

5.2. Analytical Model

We consider a particle initially bound to H_2 , with orbital velocity \mathbf{v}_0 and polar position l, θ measured in the RF of H_2 just prior to the merger. For reaching an analytical solution for the double scattering kick energy ΔE_{DS} , we now work from the orbital picture shown in Figure 2, which serves to approximate the full orbital trajectory of the particle. Following this picture, we first model the velocity kick $\Delta \mathbf{v}$ the particle receives relative to the CM of H_2 from its 'first deflection' by H_1 . We then use this kick velocity to model the orbit of the particle through H_2 , where it undergoes its 'second deflection' by the mass of H_2 enclosed by radius ϵ . This deflection rotates the velocity vector of the particle by an angle α , resulting in a velocity change δv along the motion of the merging halos. From this deflection, we then calculate the resultant energy change $\Delta E_{DS} \sim \delta v w$, as described in Section 5.1. The components of this model will be calculated in the sections below for two merging HQ halos.

5.2.1. The 'First Deflection' by Halo H_1

The particle receives a velocity kick $\Delta \mathbf{v}$ relative to H_2 , because the CM of H_2 and the particle experience different accelerations during the merger. A numerical example is shown in the top panel of Figure 3. We can analytically estimate $\Delta \mathbf{v}$ in the impulsive limit, where one assumes the particle is not moving during the encounter (e.g. Hut 1983; Aguilar & White 1985; Cincotta et al. 1991; Funato & Makino 1999).

Using a coordinate system where H_1 is moving along the x -axis and the CM of H_2 is located at $x = 0$, the kick can now be estimated by

$$\Delta \mathbf{v} \approx \int_{-T}^{+T} \mathbf{a}(t) dt = \int_{-R}^{+R} \frac{1}{w(x)} \frac{GM_1(d)}{d(x)^3} \mathbf{d}(x) dx, \quad (9)$$

where \mathbf{a} is the acceleration the particle experiences due to H_1 , $\mathbf{d} = (d_x, d_y)$ is the separation vector between the particle and the CM of H_1 , $d = |\mathbf{d}|$ is its magnitude and w is the relative velocity between H_1 and H_2 . The distance d is simply given by $d^2 = (x - x_p)^2 + y_p^2$, where $x_p = l \cos(\theta)$ and $y_p = l \sin(\theta)$ are the x and y coordinates of the particle in the frame of H_2 , respectively. In this work, we model the orbit of the particle by assuming it is not moving during the passage of H_1 from $-l, +l$, as illustrated in Figure 2. The horizontal kick velocity Δv_x is therefore calculated by setting $R = l$. The vertical kick velocity Δv_y is not sensitive to R in the same way, and is therefore calculated from just using $R = \infty$ to simplify the expressions. The horizontal and the vertical components of the kick velocity will be calculated below.

5.2.2. Horizontal Kick Velocity Δv_x

The horizontal kick velocity Δv_x is found by integrating equation (9) from $-l$ to $+l$ using $d_x = x - x_p$,

$$\Delta v_x \approx \frac{\Phi_1(0)}{w(l)} \left(\frac{1}{1 + l' \sqrt{2} \sqrt{1 - \cos(\theta)}} - \frac{1}{1 + l' \sqrt{2} \sqrt{1 + \cos(\theta)}} \right), \quad (10)$$

where we have assumed that w equals $w(l)$ during the passage. By comparing with equation (3), we see that the expression, except for the $1/w$ term, is exactly equal to the difference in potential energy of the particle between the initial configuration, where H_1 is at $-l$, and the final configuration, where H_1 is at $+l$. This is consistent from the perspective of energy conservation, where the particle must receive a kinetic energy kick to 'compensate' for the potential energy difference $\Delta \Phi_{-l, +l}$. To illustrate this, we note that in the RF

of H_1 the kinetic energy of the particle after the merger is $E_{kin}(l) \approx w(l)\Delta v_x$ and from energy conservation the kick must therefore be $\Delta v_x \approx \Delta\Phi_{-l,+l}/w(l)$ as we also find in equation (10). The horizontal velocity kick is therefore not due to a real dynamical deflection, but it arises purely from an energy difference. This difference can be calculated exactly, and as a result our estimate for Δv_x is also relatively accurate. In practice, it is useful to approximate equation (11) by $\Delta v_x(\theta) \approx \Delta v_x(0)\cos(\theta)$, where $\Delta v_x(\theta)$ denotes the solution including the full θ dependence. Using this approximation we find

$$\Delta v_x \approx \frac{\Phi_1(0)}{w(l')} \frac{2l'}{1+2l'} \cos(\theta). \quad (11)$$

In the limit where H_1 and H_2 pass through each other with the escape velocity of H_1 this reduces to the simple form: $\Delta v_x \approx -\sqrt{2}|\Phi_1(0)|l'\cos(\theta)\sqrt{1+l'}/(1+2l')$.

5.2.3. Vertical Kick Velocity Δv_y

The vertical kick velocity Δv_y arises because the particle briefly follows an orbit in the potential of H_1 , which momentarily dominates as the two merging halos pass each other. The velocity kick Δv_y can therefore be estimated from writing down the orbital solution for a particle, with encounter velocity $\sim w$ and impact parameter $\sim l\sin(\theta)$, moving in the HQ potential of H_1 . However, there are no analytical solutions for the majority of DM density profiles, including the HQ profile (Binney & Tremaine 2008), and we must therefore use the impulsive approximation presented in equation (9). Assuming the particle is only deflected by the mass of H_1 enclosed by a sphere of radius $r = |l\sin(\theta)|$, and using $d_y = y_p$, we find

$$\Delta v_y \approx \frac{\Phi_1(0)}{w(x'_p)} \frac{2y'_p}{(1+|y'_p|)^2}, \quad (12)$$

where we have assumed that w equals $w(x'_p)$ during the passage (w at time '2' shown in Figure 2). In the limit where H_1 and H_2 pass through each other with the escape velocity of H_1 , the above expression reduces to $\Delta v_y \approx -\sqrt{2}|\Phi_1(0)|y'_p\sqrt{1+x'^2_p}/(1+|y'_p|)^2$. In contrast to the horizontal kick Δv_x , the vertical kick Δv_y arises from a real dynamical deflection, which makes it hard to estimate precisely. By comparing with simulations, we find that our above estimation for Δv_y is about a factor of ~ 1.5 too low. One reason for this is that we only include the mass of H_1 enclosed by the radius $\sim l\sin(\theta)$. However, including the full HQ profile in the integration leads to a divergent result, which clearly illustrates the limits of the impulsive approximation.

5.2.4. The 'Second Deflection' by Halo H_2

After receiving the velocity kick $\Delta \mathbf{v}$, the particle starts to move from its initial position l, θ towards the central region of H_2 , where it undergoes a 'second deflection' by the mass of H_2 enclosed by radius ϵ . This changes the velocity vector of the particle from $\mathbf{v}_1 = \mathbf{v}_0 + \Delta \mathbf{v}$ to $\mathbf{v}_2 = \mathbf{v}_1 + \delta \mathbf{v}$. To estimate the components of \mathbf{v}_2 , we first calculate the impact parameter ϵ for the deflection by H_2 , as illustrated in Figure 2. Assuming $|\tan(\theta)\Delta v_x/\Delta v_y| < 1$ we find from simple geometry

$$\epsilon = |x_p| \frac{1 - \gamma \tan(|\theta|)}{\sqrt{1 + \gamma^2}}, \quad (13)$$

where $\gamma \equiv |\Delta v_x/\Delta v_y|$. Using the relation $\alpha \approx \delta v/\Delta v$ and equation (9) to estimate δv , we can now write down an ex-

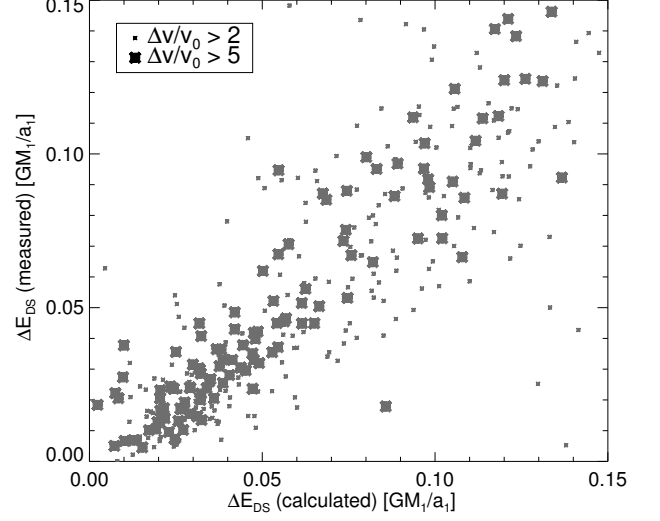


FIG. 6.— Comparison between our analytical calculation for the dynamical energy kick generated by the double scattering mechanism (x-axis) and values measured from an N-body simulation (y-axis). The analytical estimate is done using equation (17), with measured values for Δv and $w(r'_e)$ to completely focus on the mechanism itself. The two symbol sizes indicate different thresholds between the dynamical kick velocity, Δv , and the peculiar motion of the particle, v_0 , at the time of merger. As seen, our model successfully describes the kick energy from the double scattering mechanism.

pression for the deflection angle α

$$\alpha \approx \frac{2GM_2(\epsilon)}{\epsilon\Delta v^2} = \frac{2|\Phi_2(0)|}{\Delta v^2} \frac{(\epsilon/a_2)}{(1+\epsilon/a_2)^2}, \quad (14)$$

assuming that the particle is only affected by the mass of H_2 enclosed by ϵ . In the last equality we have inserted the HQ mass profile of H_2 . The deflection by H_2 conserves the length of the velocity vector of the particle in the RF of H_2 , but rotates \mathbf{v}_1 by the angle α into the new vector \mathbf{v}_2 , which therefore has coordinates given by

$$\begin{aligned} v_{2,x} &= v_{1,x}\cos\alpha + v_{1,y}\sin\alpha \\ v_{2,y} &= v_{1,y}\cos\alpha - v_{1,x}\sin\alpha. \end{aligned} \quad (15)$$

The particle will only receive a positive energy kick if $|v_{2,x}| > |v_{1,x}|$, i.e., if the kick velocity $\Delta \mathbf{v}$ and deflection angle α fulfill the inequality $|\tan(\alpha/2)\Delta v_x/\Delta v_y| < 1$ in the limit where $\Delta v \gg v_0$. From the definition of $\delta \mathbf{v} \equiv \mathbf{v}_2 - \mathbf{v}_1$ we now find the change in velocity due to the second deflection

$$\begin{aligned} |\delta v_x| &\approx |\Delta v_y\alpha| \\ |\delta v_y| &\approx |\Delta v_x\alpha| \end{aligned} \quad (16)$$

where we have assumed that $\alpha \ll 1$ and that the kick velocity dominates the motion of the particle along its new perturbed orbit, i.e. $v_1 \approx \Delta v$. The last assumption is necessary for the double scattering mechanism to work effectively.

5.2.5. Resultant Energy From the Double Scattering Mechanism

To finally calculate the dynamical kick energy ΔE_{DS} of the particle, we first assume that the second deflection by H_2 happens instantaneously, i.e., the velocity vector of the particle changes from \mathbf{v}_1 to \mathbf{v}_2 at a single point. This point occurs when the particle passes the center of H_2 at a distance $\sim \epsilon$, as shown in Figure 2. From this assumption it naturally follows that the potential energy of the particle is approximately constant during the deflection, and the change in total energy will

therefore be dominated by the change in kinetic energy. The kick energy ΔE_{DS} can therefore be estimated by

$$\Delta E_{DS}(l, \theta) \approx \frac{1}{2}(\mathbf{v}_2 + \mathbf{w}(r'_e))^2 - \frac{1}{2}(\mathbf{v}_1 + \mathbf{w}(r'_e))^2 = w(r'_e)\delta v_x, \quad (17)$$

where δv_x is the x component of the velocity change in the RF of H_2 given by equation (16), r'_e is the distance between H_1 and H_2 at the time the particle undergoes its second deflection by H_2 and $w(r'_e)$ is the corresponding relative velocity between H_1 and H_2 . In the limit where the two halos pass each other with the escape velocity of H_1 , r'_e is found by solving the differential equation $w(r) = dr/dt = \sqrt{2|\Phi_1(r)|}$. The solution for a HQ halo can be written in the form $r'_e = (3\Delta t \sqrt{2|\Phi_1(0)|}/(2a_1) + (1+l')^{3/2})^{2/3} - 1$, where $\Delta t \approx l/\Delta v$ is the time from the first deflection by H_1 to the second deflection by H_2 . For a slightly more precise estimate one has to include dynamical friction, which impacts the estimation for w . The friction will mainly play a role in slowing down the bulk of H_2 after the merger, i.e., the main change will be to the value of $w(r'_e)$. The correction will therefore factor out in equation (17), which makes it easy to include in possible future studies.

The left panel in Figure 5 shows our estimate for ΔE_{DS} , given by equation (17), as a function of the position of the particle in H_2 . One can see that our model predicts that the particles which receive a positive energy kick are all located in a cone with two wings pointing along the velocity of H_2 . Comparing with the energy kick generated by tidal fields ΔE_{TF} (illustrated in the right panel), we see that the double scattering mechanism is actually likely to be the dominating kick mechanism for particles located near the center. This is in contrast to the outer parts, where the tidal field contribution seems to be the dominating component. We confirmed this by numerical simulations.

A comparison between an N-body simulation and our analytical estimate for ΔE_{DS} is shown in Figure 6. The analytical calculation is done using equation (17), with numerical measured values for Δv and $w(r'_e)$, to completely isolate the prediction from the double scattering mechanism itself. The measured energy kick from the N-body simulation is here defined as the change in energy of the particle between the time when H_2 leaves H_1 at distance l (time '3') and the time when the particle leaves H_2 at distance l (time '5'). As seen on the figure, we find good agreement despite the difficulties in both measuring and calculating the kick energy.

6. OBSERVATIONAL SIGNATURES

The particles which have gained an energy kick through our presented mechanisms will have a relative high velocity compared to the field, and therefore have the potential of being labeled as high velocity objects. In this section, we illustrate how different the resultant velocities of the kicked particles are, compared to the virialized particles bound to H_1 .

6.1. Kick Velocity Relative to Virial Velocity

The velocity of a particle moving on a radial orbit in the potential of the target halo H_1 , is found from simple energy conservation

$$u_r(r) = \sqrt{2(E_i + \Delta E - \Phi_1(r))}, \quad (18)$$

where $u_r(r)$ is the radial velocity of the particle at distance r , E_i is the initial energy of the particle, $\Phi_1(r)$ is the radial dependent potential of H_1 and ΔE is any additional energy con-

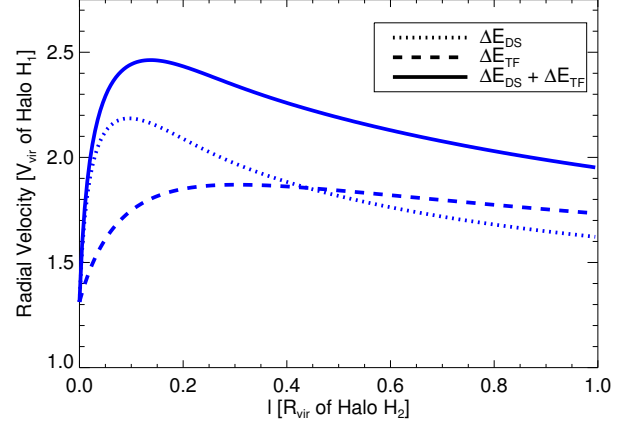


FIG. 7.— The maximum radial velocity evaluated at the virial sphere of H_1 (i.e. at distance $r = R_{1,\text{vir}}$) for a particle kicked by our presented mechanisms, as a function of its radial position l in H_2 just prior to the merger. The merger configuration is the same as the one discussed in Figure 5. The velocity curves are calculated from the maximum energy estimates shown in Figure 5 using equation (18). One can see that the dynamical mechanisms giving rise to ΔE_{TF} and ΔE_{DS} can create particles traveling with velocities $\sim 2V_{1,\text{vir}}$ at the virial sphere of their target halo.

tributions. We consider the case where $\Delta E = \Delta E_{DS} + \Delta E_{TF}$. All quantities are defined in the RF of H_1 .

Figure 7 illustrates our analytical estimate for the maximum radial velocity a dynamically kicked particle can have at the virial sphere of H_1 . The velocity is plotted in units of the virial velocity of H_1 , defined by $V_{1,\text{vir}} \equiv \sqrt{GM_{1,\text{vir}}/R_{1,\text{vir}}}$. As seen on the figure, the energy release from tidal fields and the double scattering mechanism can lead to particles with a velocity about $\sim 2V_{1,\text{vir}}$ at the virial radius of H_1 . These particles will therefore clearly stand out from the virialized part. For comparison, particles receiving no energy kicks ($\Delta E = 0$) will, in our example, instead have a velocity $\sim 1.3V_{1,\text{vir}}$. We also see that the maximum kick velocity is given to particles located around $\sim 0.1 - 0.2R_{2,\text{vir}}$ from the center of H_2 . Stars are typically located within 1–5% of the virial radius of their host halo (Kravtsov 2013), we therefore expect only the outer parts of a possible central galaxy to be effectively kicked by our presented mechanisms. The outer parts are usually populated by loosely bound stars and stellar systems, such as GCs and dwarf galaxies (Pota et al. 2013). The GCs are the only of these objects which can be seen out to cosmological distances, due to their high number and density of stars ($\sim 10^4 \text{ pc}^{-3}$), which make them a potential observable tracer of our presented mechanisms. We give an example of this in the section below.

6.2. Is HVGC-1 Kicked Through a Halo Merger?

The first detection of a high velocity globular cluster (HVGC-1) was recently reported by Caldwell et al. (2014). This high velocity object was identified as a GC from spectroscopy, and *uik* photometry and was found between GC candidates collected over several years by Keck/DEIMOS, LRIS and MMT/Hectospec (Strader et al. 2011; Romanowsky et al. 2012). The GC is located in the Virgo Cluster at a projected distance of ~ 84 kpc from M87, with a radial velocity relative to Virgo and M87 of about 2100 and 2300 km s^{-1} , respectively. The interesting question is now, how did this GC get this high velocity? As discussed in the paper by the authors, the GC could have been kicked by a binary SMBH system located in the center of M87. However, it is very un-

certain whether a GC can survive this, due to the possibility of disruption. Subhalo interactions near M87 could also be an explanation, but no subhalos have been observed in its close vicinity yet. The nature of the kick is therefore still unsolved.

The GC could have been kicked by our presented dynamical mechanisms, i.e., first by tidal fields and then by the double scattering mechanism, if it was initially bound to a DM halo merging nearly head-on with Virgo. To receive the maximum kick energy, the GC must have been located in the outskirts of its host galaxy just prior to the merger, which is not an unlikely scenario (e.g. Huxor et al. 2014; Pota et al. 2013). For a 1 : 10 mass ratio, we have shown that this merger configuration can generate objects with a radial velocity of ~ 2 times the virial velocity of the target halo at its virial radius. In the case of Virgo, this would mean a velocity of about $\sim 2 \times 1100 = 2200 \text{ km s}^{-1}$ (The virial velocity of Virgo is somewhere between $\sim 900 - 1300 \text{ km s}^{-1}$ (Strader et al. 2011)), which is consistent with the observed value for HVGC-1. We further note that HVGC-1 is observed to be hostless. This also follows from our model, since the generated kick velocity of the GC quickly separates it from its initial host galaxy. This is also seen in Figure 1. Full numerical simulations can of course be used for exploring this in more detail, including the role of encounter velocity, halo concentrations and mass profiles, impact parameter, and mass ratio. We leave that for a future study.

7. ORBITS OUTSIDE THE VIRIAL RADIUS

An interesting final question, is now what the future orbits are of the dynamically kicked particles if they leave the virial sphere of their target halo H_1 (also denoted the ‘ejector halo’ in the sections below). We study this, by solving the equation of motion for particles moving under the influence of the gravitational force of their ejector halo and the expanding cosmological background.

7.1. Equation of Motion of an Ejected Particle

The radial acceleration \ddot{r} of an ejected particle, is to first order, dominated by two terms: One from the gravitational field of the ejector halo and one from the expanding background (Nandra et al. 2012; Behroozi et al. 2013). In this approximation, the total acceleration is given by

$$\ddot{r} = -\frac{GM_1}{r^2} - H_0^2 r (\Omega_{m,0} a^{-3} - 2\Omega_{\Lambda,0}) / 2, \quad (19)$$

where M_1 is the time dependent mass of H_1 , r is the physical distance between the center of H_1 and the particle, H_0 is the Hubble parameter today, a is the scale factor (not to be confused with the HQ scale radius), and Ω is the density parameter. One can see that the force exerted by the background expansion can either be attractive *or* repulsive, depending on whether the universe is decelerating *or* accelerating, respectively. The expansion itself does therefore not imply a repulsive force (Davis et al. 2003).

The scale factor a evolves in time by the standard relation (e.g. Behroozi et al. 2013)

$$a(t) = a_{m\Lambda} \left[\sinh \left(3H_0 t \sqrt{\Omega_{\Lambda,0}} / 2 \right) \right]^{2/3}, \quad (20)$$

where $a_{m\Lambda}$ is the matter - dark energy equality scale factor given by $(\Omega_{m,0}/\Omega_{\Lambda,0})^{1/3}$. The mass of the ejector halo H_1 is time dependent as well, due to matter accretion. To include

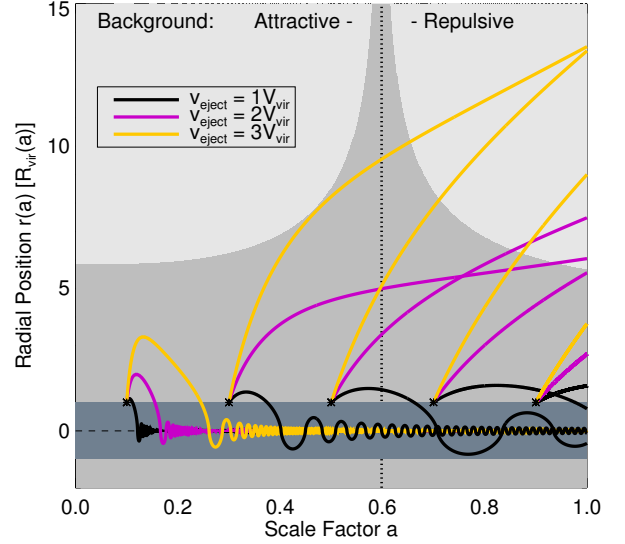


FIG. 8.— Radial position (*solid lines*) as a function of scale factor a for particles leaving the virial sphere of H_1 with velocity v_{eject} at different times (*black stars*). The *dark grey* area centered around zero shows the region inside the virial sphere of H_1 . The *grey* area shows the region where the gravitational force from the halo dominates over the force from the expanding background. In the *light grey* region the force from the background dominates. The vertical *dotted line* indicates the time when the force from the expanding background changes from being attractive (left side) to repulsive (right side), i.e., when $\Omega_{m,0} a^{-3} = 2\Omega_{\Lambda,0}$. One can see that there exists a ‘sweet spot’ around 0.3–0.5 in scale factor for ejecting particles into large orbits.

this mass evolution, we use the following empirical halo mass scaling (Wechsler et al. 2002)

$$M_1(t) = M_1(a_r) e^{\beta(z(a_r) - z(a))}, \quad (21)$$

where $M_1(a_r)$ is the mass of the halo at some reference scale factor a_r , z is the redshift and β is a constant. The constant β has been found to be in the range 0–2, using numerical simulations (Wechsler et al. 2002; McBride et al. 2009).

7.2. How Far Can an Ejected Particle Travel?

The radial motion of a high velocity particle is found by solving equation (19), including equation (20) for $a(t)$ and (21) for $M(t)$. We assume that the particle escapes the virial radius of H_1 with a velocity v_{eject} at a scale factor a_{eject} . Results are shown in Figure 8, which illustrates the particle’s radial position $r(a)$ as a function of scale factor a , for different combinations of v_{eject} and a_{eject} . The position is plotted in units of the virial radius of H_1 , which changes in time according to the defined relation $M_{vir} \equiv 4\pi \Delta_{vir} \rho_c R_{vir}^3 / 3$, where ρ_c is the time dependent critical density of the universe and Δ_{vir} is the overdensity threshold. The ejection velocity is given in units of the corresponding virial velocity, defined by $V_{vir} \equiv \sqrt{GM_{vir}/R_{vir}}$. We assume $\beta = 1$, $\Delta_{vir} = 200$, and a flat universe with $\Omega_{m,0} = 0.3$. From the orbits shown in Figure 8, we see that the maximum distance a particle can travel strongly depends on its ejection time a_{eject} , as described in the following.

A particle ejected at early times will have a long time available to travel a long distance, but will also experience a strongly increasing gravitational attraction from its ejector halo, due to mass accretion. The force from the background is also attractive at early times, and the linear dependence on the distance r makes it therefore impossible for ejected parti-

cles to become unbound (Behroozi et al. 2013). As a result of these effects, particles ejected early on will quickly return to their ejector halo and are therefore unlikely to be found freely floating around today.

A particle ejected at later times will have less time to travel away from its ejector halo, but will on the other hand experience a much smaller mass accretion, i.e. attracting force, from its ejector halo. The force from the background also changes to be repulsive at late times, which makes it even easier for late time ejected particles to escape. As seen in Figure 8, this interplay between ejection time and force terms results in a 'sweet spot' around $a \sim 0.3 - 0.5$, for ejecting particles into large orbits. The orbits also strongly depend on the ejection velocity v_{eject} . Dynamical kick mechanisms therefore play a significant role in how matter distribute around cosmological halos.

An important observation from Figure 8, is that particles ejected with only a few times the virial velocity can enter large orbits, and travel several virial radii away from their target halo. For example, a particle ejected at $a_{eject} \sim 0.5$ with velocity $v_{eject} \sim 2V_{vir}$, will be $\sim 7R_{vir}$ away from the ejector halo at present time. Including dynamical effects for estimating how far particles can reach from their target halo is therefore important, and leads to much higher limits compared to previous estimations based, e.g., on the halo collapse formalism (Mamon et al. 2004). A similar conclusion was reached by, e.g., Sales et al. (2007); Ludlow et al. (2009) using cosmological N-body simulations.

8. CONCLUSIONS

We provide an explanation for how high energy particles are created in halo mergers, by introducing a model which includes a double scattering mechanism. The mechanism is a process where an incoming halo particle undergoes two subsequent gravitational deflections during the merger, where the first is by the mass of the target halo and the second is by the mass of the particle's original host halo. The particle can receive a significant energy kick from this process, because the two frames of deflection, i.e. the two halos, move relative to each other during the merger. The amount of energy gener-

ated through this mechanism, is comparable to a well known energy contribution from tidal fields. The mechanism is therefore playing a significant role in how energy is distributed in halo mergers. To our knowledge, the double scattering mechanism has not been characterized in this context before, despite its great importance especially for explaining the origin of high velocity particles.

From our presented model, we derive analytically the kick energy a given particle receives from tidal fields and the double scattering mechanism, as a function of its position in its original host halo just prior to the merger. In the case of a 1 : 10 head-on merger, we estimate that the largest energy kick is about $0.3 - 0.4\Phi_1(0)$, and is given to particles located at around $\sim 0.1 - 0.2R_{vir}$ from the original host halo center. We find this to be in agreement with numerical simulations.

By converting kick energy to velocity, we illustrate that our presented mechanisms can kick objects to a resultant velocity ~ 2 times the virial velocity of the target halo measured at its virial sphere. This motivates us to suggest, that the high velocity of the recently discovered globular cluster HVG-1 (Caldwell et al. 2014), can be explained by a halo merger, i.e., that the energy kick is generated by tidal fields and the double scattering mechanism. We believe this serves as a more natural explanation compared to other proposed ideas, including three-body interactions with a binary SMBH system in M87. Cosmological simulations also support this (Sales et al. 2007).

Finally, from solving the equation of motion of a dynamically kicked particle in an expanding universe, we find a 'sweet spot' around a scale factor of $0.3 - 0.5$ for ejecting particles into large orbits. These orbits can easily reach beyond ~ 5 virial radii from the target halo, which is significantly longer than previous estimates based on halo collapse models (e.g. Mamon et al. 2004). This illustrates the importance of including dynamical interactions for describing the outer regions of cosmological halos.

It is pleasure to thank S. Hansen, T. Brinckmann, J. Zavala, R. Wojtak, M. Sparre, J. Hjorth, S. Pedersen, J. Fynbo, J. Zabl, K. Finlator and S. Hoenig for comments and helpful discussions. The Dark Cosmology Centre is funded by the Danish National Research Foundation.

REFERENCES

- Abadi, M. G., Navarro, J. F., & Steinmetz, M. 2009, *ApJ*, 691, L63
 Aguilar, L. A., & White, S. D. M. 1985, *ApJ*, 295, 374
 Behroozi, P. S., Loeb, A., & Wechsler, R. H. 2013, *Journal of Cosmology and Astroparticle Physics*, 6, 19
 Bekenstein, J. D. 1973, *ApJ*, 183, 657
 Bertschinger, E. 1985, *ApJS*, 58, 39
 Binney, J., & Tremaine, S. 2008, *Galactic Dynamics: Second Edition* (Princeton University Press)
 Blaauw, A. 1961, *Bull. Astron. Inst. Netherlands*, 15, 265
 Boylan, C., Li, Y., Fan, X. L., & Heng, I. S. 2014, *ArXiv e-prints*
 Bromley, B. C., Kenyon, S. J., Geller, M. J., Barcikowski, E., Brown, W. R., & Kurtz, M. J. 2006, *ApJ*, 653, 1194
 Brown, W. R., Cohen, J. G., Geller, M. J., & Kenyon, S. J. 2012, *ApJ*, 754, L2
 Brown, W. R., Geller, M. J., & Kenyon, S. J. 2014, *ApJ*, 787, 89
 Burrows, A., & Hayes, J. 1996, in *American Institute of Physics Conference Series*, Vol. 366, *High Velocity Neutron Stars*, ed. R. E. Rothschild & R. E. Lingens, 25-37
 Burrows, A., Livne, E., Dessart, L., Ott, C. D., & Murphy, J. 2007, *ApJ*, 655, 416
 Caldwell, N., Strader, J., Romanowsky, A. J., Brodie, J. P., Moore, B., Diemand, J., & Martizzi, D. 2014, *ApJ*, 787, L11
 Carucci, I. P., Sparre, M., Hansen, S. H., & Joyce, M. 2014, *ArXiv e-prints*
 Chandrasekhar, S. 1943, *ApJ*, 97, 255
 Chapman, S. C., et al. 2007, *ApJ*, 662, L79
 Cincotta, P. M., Muzzio, J. C., & Nunez, J. A. 1991, *Celestial Mechanics and Dynamical Astronomy*, 52, 263
 Dalal, N., Lithwick, Y., & Kuhlen, M. 2010, *ArXiv e-prints*
 Davies, M. B., King, A., Rosswog, S., & Wynn, G. 2002, *ApJ*, 579, L63
 Davis, T. M., Lineweaver, C. H., & Webb, J. K. 2003, *American Journal of Physics*, 71, 358
 Drisko, R. M. 1955, PhD thesis, CARNEGIE-MELLON UNIVERSITY.
 Eddington, A. S. 1916, *MNRAS*, 76, 572
 Fakhouri, O., Ma, C.-P., & Boylan-Kolchin, M. 2010, *MNRAS*, 406, 2267
 Fitchett, M. J. 1983, *MNRAS*, 203, 1049
 Fong, W., et al. 2013, *ApJ*, 769, 56
 Funato, Y., & Makino, J. 1999, *ApJ*, 511, 625
 Gal-Yam, A., Maoz, D., Guhathakurta, P., & Filippenko, A. V. 2003, *AJ*, 125, 1087
 Gualandris, A., Portegies Zwart, S., & Sipiro, M. S. 2005, *MNRAS*, 363, 223
 Guenou, L., et al. 2012, *A&A*, 537, A64
 Gvaramadze, V. V., Gualandris, A., & Portegies Zwart, S. 2009, *MNRAS*, 396, 570
 Hansen, S. H., Egli, D., Hollenstein, L., & Salzmann, C. 2005, *New Astronomy*, 10, 379
 Heggie, D. C. 1975, *MNRAS*, 173, 729
 Hernquist, L. 1990, *ApJ*, 356, 359

- , 1992, *ApJ*, 400, 460
- Hills, J. G. 1988, *Nature*, 331, 687
- Hjorth, J., & Williams, L. L. R. 2010, *ApJ*, 722, 851
- Hut, P. 1983, *ApJ*, 268, 342
- Huxor, A. P., et al. 2014, *MNRAS*, 442, 2165
- Janka, H.-T. 2012, *Annual Review of Nuclear and Particle Science*, 62, 407
- Joyce, M., Marcos, B., & Sylos Labini, F. 2009, *MNRAS*, 397, 775
- Kochanek, C. S. 1994, *ApJ*, 422, 508
- Kravtsov, A. V. 2013, *ApJ*, 764, L31
- Ludlow, A. D., Navarro, J. F., Springel, V., Jenkins, A., Frenk, C. S., & Helmi, A. 2009, *ApJ*, 692, 931
- Lynden-Bell, D. 1967, *MNRAS*, 136, 101
- Majewski, S. R., et al. 2007, *ApJ*, 670, L9
- Mamon, G. A., Sanchis, T., Salvador-Solé, E., & Solanes, J. M. 2004, *A&A*, 414, 445
- McBride, J., Fakhouri, O., & Ma, C.-P. 2009, *MNRAS*, 398, 1858
- Mo, H., van den Bosch, F. C., & White, S. 2010, *Galaxy Formation and Evolution*
- Moore, B., Katz, N., Lake, G., Dressler, A., & Oemler, A. 1996, *Nature*, 379, 613
- Nandra, R., Lasenby, A. N., & Hobson, M. P. 2012, *MNRAS*, 422, 2931
- Ogorodnikov, K. F. 1957, *Soviet Ast.*, 1, 748
- Peñarrubia, J., Kuposov, S. E., & Walker, M. G. 2012, *ApJ*, 760, 2
- Peng, E. W., et al. 2011, *ApJ*, 730, 23
- Pietilä, H., Heinämäki, P., Mikkola, S., & Valtonen, M. J. 1995, *Celestial Mechanics and Dynamical Astronomy*, 62, 377
- Pontzen, A., & Governato, F. 2013, *MNRAS*, 430, 121
- Pota, V., et al. 2013, *MNRAS*, 428, 389
- Prada, F., Klypin, A. A., Cuesta, A. J., Betancort-Rijo, J. E., & Primack, J. 2012, *MNRAS*, 423, 3018
- Presotto, V., et al. 2014, *A&A*, 565, A126
- Price-Whelan, A. M., Hogg, D. W., Johnston, K. V., & Hendel, D. 2014, *ArXiv e-prints*
- Read, J. I., Wilkinson, M. I., Evans, N. W., Gilmore, G., & Kleyna, J. T. 2006, *MNRAS*, 366, 429
- Redmount, I. H., & Rees, M. J. 1989, *Comments on Astrophysics*, 14, 165
- Romanowsky, A. J., Strader, J., Brodie, J. P., Mihos, J. C., Spitler, L. R., Forbes, D. A., Foster, C., & Arnold, J. A. 2012, *ApJ*, 748, 29
- Sales, L. V., Navarro, J. F., Abadi, M. G., & Steinmetz, M. 2007, *MNRAS*, 379, 1475
- Sand, D. J., et al. 2011, *ApJ*, 729, 142
- Sanderson, R. E., Helmi, A., & Hogg, D. W. 2014, in *IAU Symposium*, Vol. 298, *IAU Symposium*, ed. S. Feltzing, G. Zhao, N. A. Walton, & P. Whitelock, 207–212
- Shakeshaft, R., & Spruch, L. 1979, *Reviews of Modern Physics*, 51, 369
- Sigurdsson, S., & Phinney, E. S. 1993, *ApJ*, 415, 631
- Sparre, M., & Hansen, S. H. 2012a, *Journal of Cosmology and Astroparticle Physics*, 7, 42
- , 2012b, *Journal of Cosmology and Astroparticle Physics*, 10, 49
- Spergel, D. N., & Hernquist, L. 1992, *ApJ*, 397, L75
- Springel, V. 2005, *MNRAS*, 364, 1105
- Strader, J., et al. 2011, *ApJS*, 197, 33
- Teyssier, M., Johnston, K. V., & Shara, M. M. 2009, *ApJ*, 707, L22
- Thomas, L. H. 1927, *Royal Society of London Proceedings Series A*, 114, 561
- Tunnicliffe, R. L., et al. 2014, *MNRAS*, 437, 1495
- Wechsler, R. H., Bullock, J. S., Primack, J. R., Kravtsov, A. V., & Dekel, A. 2002, *ApJ*, 568, 52
- Wetzel, A. R. 2011, *MNRAS*, 412, 49
- Willman, B., Governato, F., Wadsley, J., & Quinn, T. 2004, *MNRAS*, 355, 159
- Yu, Q., & Tremaine, S. 2003, *ApJ*, 599, 1129
- Zhao, H., Johnston, K. V., Hernquist, L., & Spergel, D. N. 1999, *A&A*, 348, L49
- Zheng, Z., et al. 2014, *ApJ*, 785, L23
- Zwicky, F. 1951, *PASP*, 63, 61